European Journal of Medicinal Chemistry 193 (2020) 112206

Contents lists available at ScienceDirect

European Journal of Medicinal Chemistry

journal homepage: http://www.elsevier.com/locate/ejmech

Research paper

Development of potent inhibitors of the human microsomal epoxide hydrolase

Bogdan Barnych [a], Nalin Singh [a], Sophie Negrel [a], Yue Zhang [b], Damien Magis [a], Capucine Roux [a], Xiude Hua [a, e], Zhewen Ding [a], Christophe Morisseau [a], Dean J. Tantillo [b], Justin B. Siegel [b, c, d], Bruce D. Hammock [a, *]

[a] Department of Entomology and Nematology, UCD Comprehensive Cancer Center, University of California Davis, Davis, CA, 95616, United States
[b] Department of Chemistry, University of California Davis, Davis, CA, 95616, United States
[c] Department of Biochemistry and Molecular Medicine, University of California Davis, Davis, CA, 95616, United States
[d] Genome Center, University of California Davis, Davis, CA, 95616, United States
[e] College of Plant Protection, Nanjing Agricultural University, Nanjing, 210095, China

ARTICLE INFO

Article history:
Received 23 January 2020
Received in revised form
3 March 2020
Accepted 3 March 2020
Available online 13 March 2020

Keywords:
Microsomal epoxide hydrolase
Enzyme inhibitors
2-Alkylthio acetamide series
Molecular docking
Amides
Benzyl-thio

ABSTRACT

Microsomal epoxide hydrolase (mEH) hydrolyzes a wide range of epoxide containing molecules. Although involved in the metabolism of xenobiotics, recent studies associate mEH with the onset and development of certain disease conditions. This phenomenon is partially attributed to the significant role mEH plays in hydrolyzing endogenous lipid mediators, suggesting more complex and extensive physiological functions. In order to obtain pharmacological tools to further study the biology and therapeutic potential of this enzyme target, we describe the development of highly potent 2-alkylthio acetamide inhibitors of the human mEH with IC_{50} values in the low nanomolar range. These are around 2 orders of magnitude more potent than previously obtained primary amine, amide and urea-based mEH inhibitors. Experimental assay results and rationalization of binding through docking calculations of inhibitors to a mEH homology model indicate that an amide connected to an alkyl side chain and a benzyl-thio function as key pharmacophore units.

© 2020 Elsevier Masson SAS. All rights reserved.

1. Introduction

The microsomal epoxide hydrolase (mEH, EPHX1, E.C. 3.3.2.9) is a mammalian α/β-fold hydrolase enzyme, expressed in almost all tissues. It is mainly localized in the endoplasmic reticulum (ER) of eukaryotic cells [1]. However, it can come off the ER, exit the cell and appear in the blood where it is termed the preneoplastic antigen [2] and has been explored as a marker for liver cancer and hepatitis. It catalyzes the hydration of epoxides to the corresponding diols. It hydrolyzes a wide variety of substrates, ranging from most mono-substituted epoxides to several gem- and cis-di-substituted epoxides. *trans*-Disubstituted and trisubstituted epoxides are often poor substrates or even act as competitive inhibitors of mEH [3]. The mEH also seems to be inactive on tetrasubstituted epoxides. Recently, oxetanes were showed to be hydrolyzed by mEH *in vitro* [4,5]. The mEH metabolizes xenobiotics both *in vitro* and *in vivo*, where it plays either detoxification or bioactivation roles depending on the particular xenobiotic [3]. Polymorphism and association studies suggest a link between the enzyme and some diseases such as preeclampsia, hypercholanemia and cancer [1].

Since endogenous epoxy-fatty acids (EpFAs) are relatively poor substrates for mEH compared to soluble epoxide hydrolase (sEH), *in vitro*, the involvement of mEH in regulation of these beneficial lipid mediators was considered to be only marginal. Recently, however, using genetic KO mice it has been shown that mEH can play a significant role in the hydrolysis of EpFAs, such as the epoxyeicosatrienoic acids (EETs), *in vivo* [6]. In addition, inhibition of mEH seems to complement inhibition of sEH in improving post-ischemic functional recovery in murine hearts, suggesting that mEH inhibition may also have promising therapeutic potential.

The first reported mEH inhibitors were alternate substrates that were poorly turned over [7–9]. Previously, we showed that primary ureas, amides and amines can inhibit mEH with a single digit

* Corresponding author.
E-mail address: bdhammock@ucdavis.edu (B.D. Hammock).

https://doi.org/10.1016/j.ejmech.2020.112206
0223-5234/© 2020 Elsevier Masson SAS. All rights reserved.

micromolar range potency [10]. Later, we developed stable inhibitors of the rat mEH with IC_{50} in the high nanomolar range [11]. In order to better understand the biological roles of mEH and evaluate the therapeutic potential of mEH inhibition, we aimed to develop novel and highly potent (low nanomolar range IC_{50}) chemical inhibitors of the human mEH.

2. Results and discussion

Previously, a series of differently substituted 2-(alkylthio)propanamides was tested on the human mEH but most of the compounds were not potent inhibitors of the enzyme [12]. In this study, some newly derived 2-(alkylthio)propanamides **2**–**5** displayed significantly improved inhibitory potencies, though none of them was more potent than the reference compound **1**. Since bromoacetamides and thiols are readily available either directly from commercial sources or synthetically, optimization for potency of the 2-alkylthio acetamide class of compounds seemed very attractive in terms of potential library size and its accessibility. Therefore, the effect of substituents at the α position to the amide function and at the sulfur atom on the human mEH inhibitory potency was studied. Since the reaction between α-bromo amides and thiols often proceeds to completion, as confirmed by TLC, and the starting materials do not inhibit mEH (Tables SI–1, supplementary information), most of the initial screenings were performed using crude reaction mixtures. The best inhibitors were then resynthesized, purified, characterized and tested in the pure form. As can be seen from Table 1 very similar results were obtained for crude reaction mixtures and pure products (**6**, **7**, **16**, **17**, **23**, **24**), validating this approach.

First, the effect of the alkyl/aryl-thio substituent at the α-position of phenylacetamide on the human mEH inhibition was investigated. A range of phenylacetamides with either adamantylthio-, arylthio- or benzylthio-substituents at the α-carbon (**10**–**17**) were prepared and tested (Table 1). Adamantylthio- (**10**) and arylthio-substituted (**11**) phenylacetamides were, in general, poorer inhibitors of the human mEH compared to the benzylthioacetamides (**12**–**17**), probably due to steric factors. Compounds **16** and **17** were then obtained in pure form, and were five and two-fold more effective, respectively, than the most potent inhibitors developed at that point (**6**, **7**).

Next, the effect of the different α-alkyl substituents (**18**–**28**) on the mEH inhibitory potency of substituted primary amides was explored. For the series of compounds with the thioether substituent fixed to the *meta*-trifluoromethyl benzylthiol (**4, 17**–**19, 24**–**28**), the inhibitory potency increased in the range Me (**4**) < *n*-Pr (**18**) < *n*-Bu (**19**) and was almost two orders of magnitude higher for **19** than for **4**. Replacing the n-alkyl chain by the branched chain decreased the IC_{50} values even further, with *i*-Pr side chain (**24**) being more potent than *n*-Bu (**19**). Among the branched side chains tested the cyclopentyl substituent (**27**) proved to have the largest impact on potency and shifted the IC_{50} value down to 16 nM. Replacement of the alkyl by a second *meta*-trifluoromethyl benzylthio-function resulted in compound **25** with an IC_{50} of 23 nM, comparable to compounds **24**, **27** and **28**. Since replacement of the branched alkyl side chain with *meta*-trifluoromethyl benzylthio-substituent did not have any major effect on inhibitory potency, we tested if the same is true for the replacement of the first *meta*-trifluoromethyl benzylthio-function (**4, 17**–**19, 24**–**28**) with alkyl function (**30**). Thus, 2,2-dicyclohexylacetamide **30** has been synthesized from the commercially available 2,2-dicyclohexylacetic acid. Surprisingly, amide **30** was almost three orders of magnitude less potent than the structurally related compound **28**, pointing out the importance of benzylthio substituent for inhibitory potency. Interestingly, reduction of the amide function (**30**) to corresponding primary amine (**31**) resulted in almost one order of magnitude potency increase (Table 1).

Since thioethers are relatively unstable *in vivo* and could be easily oxidized to corresponding sulfoxides or sulfones by means of either the cytochrome P450 [13] or flavin monooxygenase (FMO) [14] family of enzymes, we tested the effect this potential oxidation products have on the inhibitory potency. Oxidation of **6** and **7** to corresponding sulfoxides **8** and **9** (mixtures of epimers at the sulfur stereogenic center) decreased their inhibitory potency by approximately two orders of magnitude (Table 1). Although the rates of thioether oxidation by CYP450 or FMO depend on stereochemical characteristics of a particular compound, the result suggests that it would be desirable to replace thioether by metabolically more stable function. Considering that 2,3-diphenylpropanamide **29** is a better inhibitor of mEH to its structurally close thio-analogue **131** (Table 4), it is likely that methylene group may serve a role of a metabolically more stable replacement function for thioether. This result is also congruent with our previous results [11], however the validity of this assumption for benzylthio-series of compounds will need to be tested (Scheme 1).

After optimization of the alkyl side chain, the attention was drawn to the optimization of the thioether substituent. Thus, 2-cyclopentyl-2-mercaptoacetamide **33** was synthesized from commercially available 2-cyclopentylacetyl chloride (Scheme 2) and, interestingly, it was a significantly more potent inhibitor than the parent 2-bromo-2-cyclopentylacetamide (**33** versus **32**). Following alkylation of mercaptoacetamide **33** with various commercially available aryl bromides, the mEH inhibitory potency of the reaction mixtures was tested, and the most potent compounds were then resynthesized, purified, characterized and the inhibitory potency of the pure compounds was tested (Table 2).

As seen in Table 2, heteroaromatic substituents mainly reduced inhibitory potency of the compounds (**34**–**37**). Compound **38** with a naphthalen-2-ylmethylthio substituent was just slightly less potent compared to the best inhibitor **27** made so far. Introduction of the polar functional groups at the *para* or *meta* positions of the benzyl substituent had mainly negative effect on the inhibitory potency (**39**–**52**), except for the nitro group in the *meta* position (**51**). Compounds with difluorobenzylthio-sidechains **53**–**54**, as well as cyclohexylmethylthio-sidechain **55** were relatively poor inhibitors of the human mEH. Finally, compounds with bulky/lipophilic substituents in meta/*para* positions on phenyl ring **56**–**62** showed the highest inhibitory potency against the human mEH. The most potent inhibitor was 2-((3,5-bis(trifluoromethyl)benzyl)thio)-2-cyclopentylacetamide **62** which had an IC_{50} of 2.2 nM. It is worth noting that replacement of the 3-(trifluoromethyl)benzyl substituent in **28** with a homologous 3-(trifluoromethyl)phenethyl substituent (**64**) did not have any effect on inhibitory potency while its replacement with 1-(3-(trifluoromethyl)phenyl)ethyl decreased the IC_{50} by over 3 times, bringing it to 4.7 nM (**63**).

A second assay, based on a radioactive substrate and not fluorescence [15], was conducted to validate the inhibitory potential of the most potent compound **62** for two reasons. Firstly, the IC_{50} obtained approached the assay limit (1.95 nM) to effectively distinguish potent inhibitors, and hence could have a degree of uncertainty associated with it. Secondly, an alternative means of IC_{50} determination would help verify that the observed potency was intrinsic and independent of the assay employed. The experiment yielded an IC_{50} of 0.94 nM, reinforcing the observation that **62** is the most potent mEH inhibitor in this series.

Additionally, a broad panel of commercially available compounds together with some in house synthesized chemicals were screened to find new structural leads. The results of those preliminary screens are reported in Tables 3–5 and Table SI-1 (in supplementary information). Since simple primary amines like

Table 1
Effect of the α-substituents on the human mEH inhibitory potency of acetamides.

#	Structure	IC_{50}, nM	#	Structure	IC_{50}, nM
1 NSPA	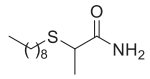	1580 ± 600	**17**	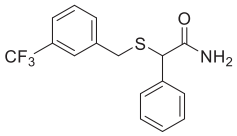	250 140[a]
2	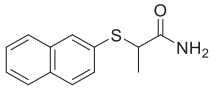	10400	**18**	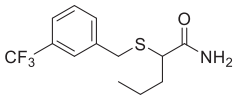	150
3	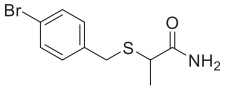	8800	**19**	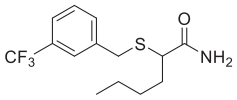	29
4	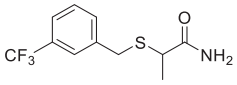	1600	**20**	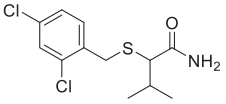	140
5	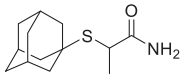	5400	**21**	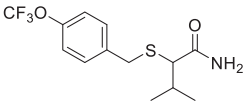	670
6	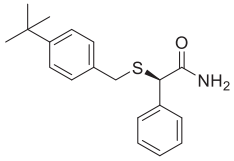	680 640[a]	**22**	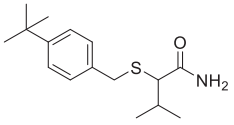	430
7	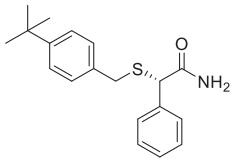	480 640[a]	**23**	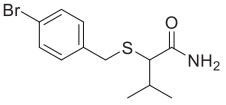	110 100[a]
8	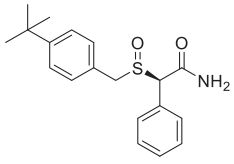	42000	**24**	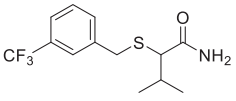	25 88[a]
9	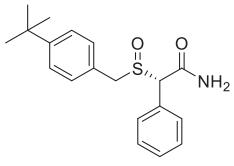	53000	**25**	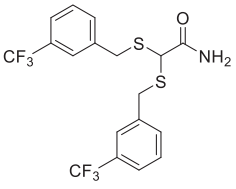	23
10	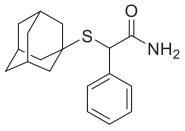	20000	**26**	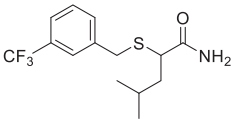	28
11	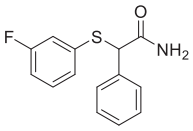	3100	**27**	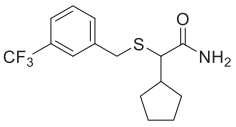	16

(*continued on next page*)

Table 1 (*continued*)

#	Structure	IC_{50}, nM	#	Structure	IC_{50}, nM
12	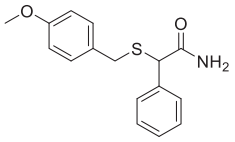	4500	**28**	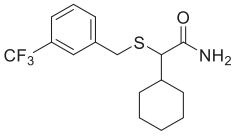	19
13	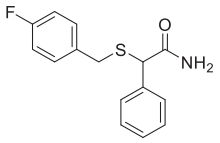	2000	**29**	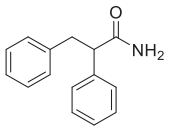	28000
14	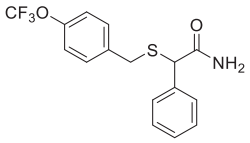	500	**30**	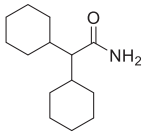	16000
15	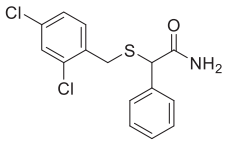	280	**31**	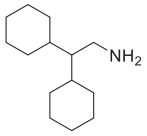	2200
16	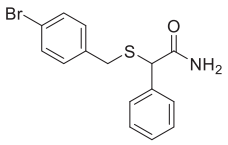	110 110[a]	**32**	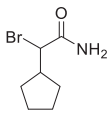	>50000

[a] Reaction mixture value.

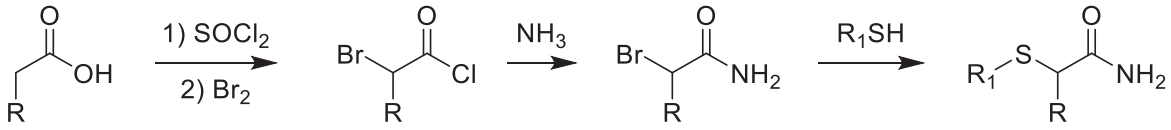

Scheme 1. General scheme for the synthesis of compounds **1**–**28** from Table 1.

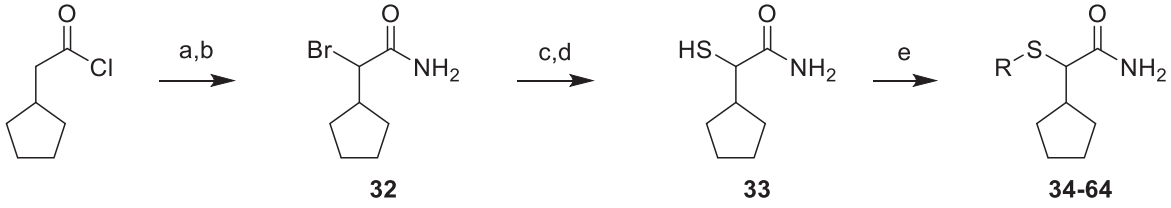

Scheme 2. Synthesis of compounds **33** and **34**–**64**. a) Br_2, 50 °C; b) NH_4OH, 0 °C; c) KSAc, DMF, 60 °C; d) NaOH, MeOH; e) RBr, K_2CO_3, DMF.

dodecyl amine are relatively good mEH inhibitors and can be easily functionalized at the nitrogen position, the effect of substitution at nitrogen was first studied (Table 3). Unfortunately, none of the synthesized dodecyl amine derivatives **66**–**76** have higher potency on mEH than the parent dodecyl amine **65**. Though, N-dodecylformamide **66** and N-dodecyl-1,1,1-trifluoromethanesulfonamide **71** have potencies similar to the parent amine. Interestingly, replacement of the formyl function with larger acyl homologues resulted in compounds **72**–**76** that are weak inhibitors of the mEH at low concentrations but cause an apparent increase of the enzyme activity at higher concentrations. Similar activation of the mEH enzymatic activity has been observed previously for other compounds [16]. Although not completely understood, this activation may be due to the binding to an allosteric site which increases catalytic activity of mEH or a change in access of the substrate to the catalytic site. Among the other compounds tested, almost all of them were poor inhibitors of human mEH (IC_{50} > 50 μM, Table 4 and Table SI-1 in supplementary information) except for 1,3-diphenylpropan-2-amine **138** and its formamide **137** that inhibited 50% of mEH activity at 1.9 and 3.3 μM

Table 2
Effect of the α-alkylthio substituent on the mEH inhibitory potency of 2-cyclopentyl-acetamides.

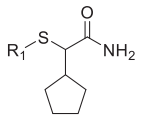

#	R_1	IC_{50}, nM	#	R_1	IC_{50}, nM
33	H	7650	**49**	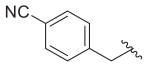	2100
34	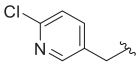	1466	**50**	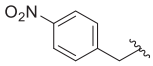	315
35	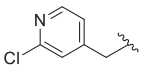	493	**51**	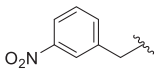	32
36	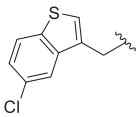	1100	**52**	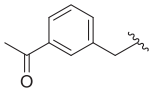	384
37	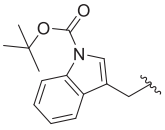	500	**53**	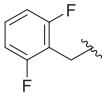	441
38	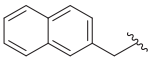	33	**54**	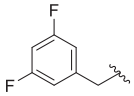	399
39	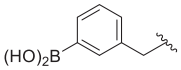	4940	**55**	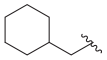	773
40	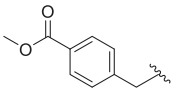	2900	**56**	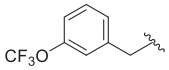	26
41	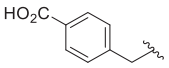	6600	**57**	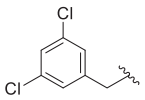	11
42	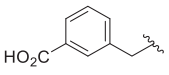	839	**58**	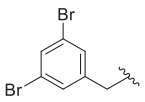	9
43	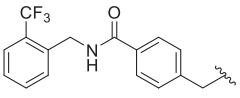	422	**59**	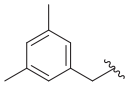	18
44	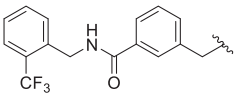	433	**60**	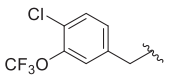	10
45	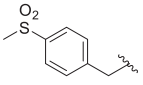	6960	**61**	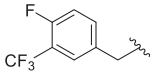	10.1

(*continued on next page*)

Table 2 (*continued*)

#	R_1	IC_{50}, nM	#	R_1	IC_{50}, nM
46	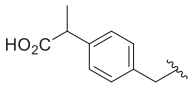	899	**62**	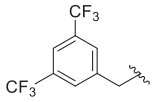	2.2
47	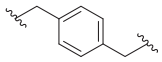	600	**63**	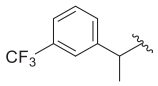	4.7
48	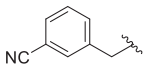	193	**64**	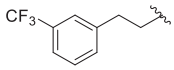	14

Table 3
Effect of N-substitution on the mEH inhibition by primary amides.

#	Structure	IC_{50}, μM	Inhibition at 100 μM, %
65		12.9	83
66		15.1	80
67		61.3	67
68		>100	5
69		>100, 100[a]	0, 50[a]
70		>100	40, 25[a]
71	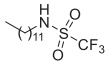	14.7, 12.5[a]	65, 98[a]
72		>100	33, 0[a,b]
73	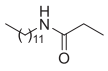	>100	-[b]
74	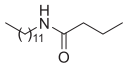	>100	-[b]
75	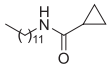	>100	-[b]
76	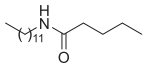	>100	−15[b]

[a] Reaction mixture value.
[b] increase in mEH activity.

respectively. Although, the inhibitory potencies of **137** and **138** were almost an order magnitude higher than the initial dodecylamine **65**, further structural optimization of those hits was considered to be difficult and low throughput due to the scarcity of the related amines, and thus was not followed here. Table 5 shows data on mEH inhibitory potency of some oxetanes. As can be seen, most of the oxetanes tested did not inhibit mEH except for **144** and **146** that inhibited 50% of mEH activity at 72 and 51 μM respectively. Considering that oxetanes could be converted to corresponding diols by mEH [4,5], it seems reasonable to assume that **144** and **146** act as slow turnover substrates, similar to the earlier reported cyclohexene oxide, 1,1,1-trichloropropane-2,3-epoxide and sterically hindered cyclodiene epoxides [7–9].

Next, homology modeling was performed to predict the mEH protein structure and docking studies were conducted with compounds **4, 27** and the most potent structure **62** to predict the preferred binding modes of the inhibitors to the active site of mEH. To ensure the charge assignments for each atom of **62** were reasonable, atomic charges were calculated with the CHelpG [17] method in GAUSSIAN09 [18]. The charges of the ligand were then assigned to each atom and further prepared for docking. 2500 docking runs were performed, and 38 structures were retained after filtering. Two major binding modes (poses) were predicted; these are shown in Fig. 1. The interface energy for the preferred pose of **62** is predicted to be −19.85 (Rosetta energy unit, REU).

For both poses, as expected [19], D226, Y299 and Y374 hydrogen bond with the amide group of the inhibitor as constrained (e.g., Fig. 2, left). For pose 1 (Fig. 1, left), a π−π stacking interaction between **62** and W227 was calculated (Fig. 2, right), which likely contributes to favorable binding. The orientation of pose 2 (Fig. 1, right) is consistent with the two dominant poses predicted for molecule **27** (*vide infra*). Other interactions, including S-π interactions, were predicted in some docking runs (see SI for details). To assess the inherent energies for the inhibitor conformers in poses 1 and 2, these structures were extracted and optimized with DFT (SMD(water)- ωB97XD/6-31+G(d,p)) [20,21,22]. The conformer in pose 1 is predicted to be 2.4 kcal/mol lower in energy than the conformer in pose 2, suggesting that both are energetically accessible.

To investigate the difference in mEH inhibitory potency with different alkyl substituents alpha to the acetamide, docking simulations for molecules **4** and **27** were conducted since the experimental result shows that the latter is 100-fold more potent than the former. Among the 2500 poses generated in the docking runs for **27**, 43 poses passed the filters mentioned above. The majority of these poses fall into the two binding modes shown in Fig. 3A. Among the 2500 poses for **4**, 41 poses passed the filters. Poses of **4** are less converged than those for **27** (see SI for detail), which may be a result of the methyl group not filling the space in the active site as well as does the cyclopentyl group (see Fig. 3B). Interface energies for the two molecules are noticeably different, with the values of −14.85 and −19.68 predicted for **4** and **27**, respectively, consistent with the difference in inhibition. The two predicted preferred binding orientations of molecule **27** (Fig. 3A) are consistent with pose 2 of molecule **62** (Fig. 3C). Each of the trifluoromethyl groups of **62** corresponds to one of the two poses of molecule **27**.

Table 4
Inhibition data for the compounds that showed more than 10% inhibition of mEH but less than 50% at 50 μM concentration. Blanc reactions did not inhibit mEH.

#	Structure	Inhibition at 50 μM, %	#	Structure	Inhibition at 50 μM, %
77	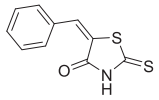	60[a]	**108**	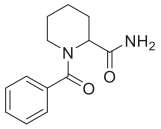	15
78	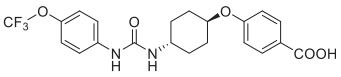	25	**109**	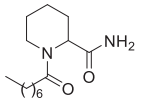	12
79	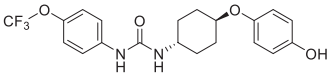	30	**110**	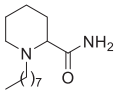	33
80	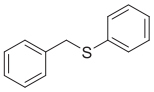	40	**111**	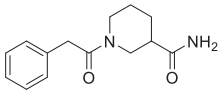	18
81	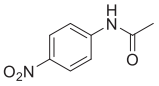	40	**112**	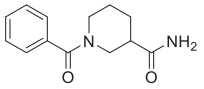	15
82	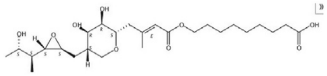	38	**113**	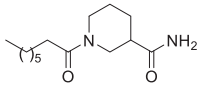	22
83	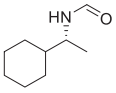	30	**114**	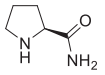	12
84	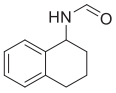	15	**115**	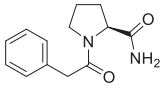	29
85	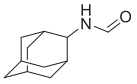	20	**116**	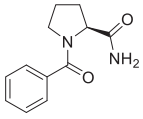	17
86	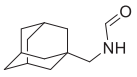	45	**117**	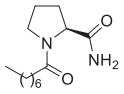	45
87	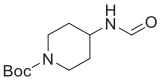	20	**118**	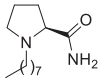	24
88	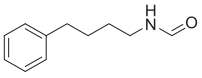	20	**119**	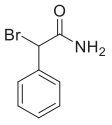	10
89	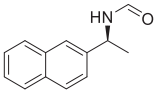	20	**120**	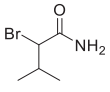	31
90	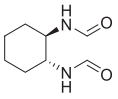	25	**121**	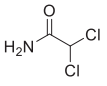	23
91	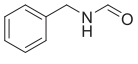	24	**122**	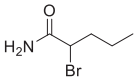	11

(*continued on next page*)

Table 4 (*continued*)

#	Structure	Inhibition at 50 μM, %	#	Structure	Inhibition at 50 μM, %
92	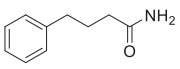	15	**123**	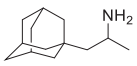	36
93	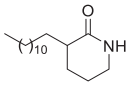	41	**124**	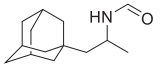	41
94	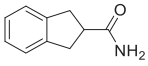	31	**125**	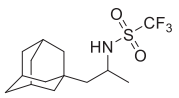	38
95	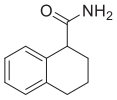	26	**126**	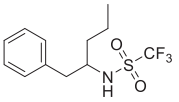	19
96	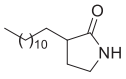	47	**127**	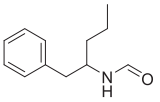	24
97	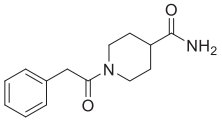	32	**128**	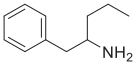	19
98	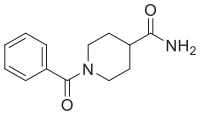	20	**129**	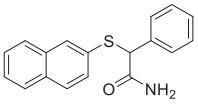	37
99	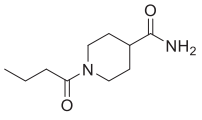	31	**130**	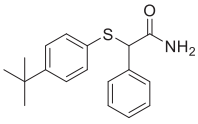	36
100	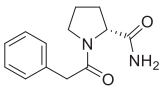	25	**131**	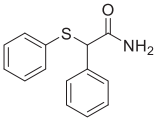	34
101	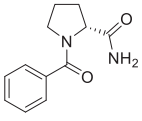	18	**132**	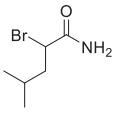	35
102	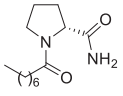	25	**133**	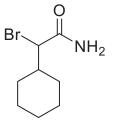	37
103	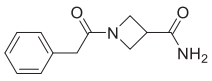	15	**134**	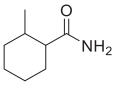	IC_{50} = 87 μM[b]
104	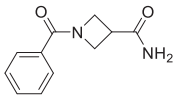	11	**135**	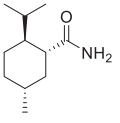	IC_{50} = 55 μM[b]
105	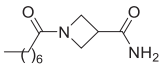	15	**136**	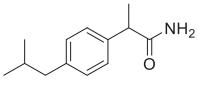	IC_{50} = 96 μM[b]

Table 4 (*continued*)

#	Structure	Inhibition at 50 μM, %	#	Structure	Inhibition at 50 μM, %
106	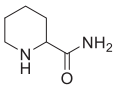	17	**137**	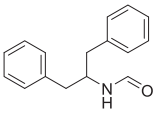	IC_{50} = 3.3 μM
107	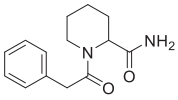	16	**138**	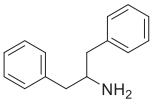	IC_{50} = 1.9 μM

[a] IC_{50} = 33.6 μM [b] apparent increase in mEH activity at low concentrations.

Table 5
mEH inhibition by oxetanes.

#	Structure	IC_{50}, μM	#	Structure	IC_{50}, μM
139		>100	**144**	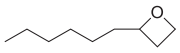	72
140	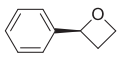	>100	**145**		>100
141	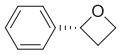	>100	**146**		51
142	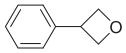	>100	**147**	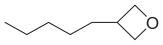	>100
143	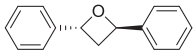	>100	**148**	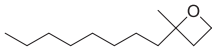	>100

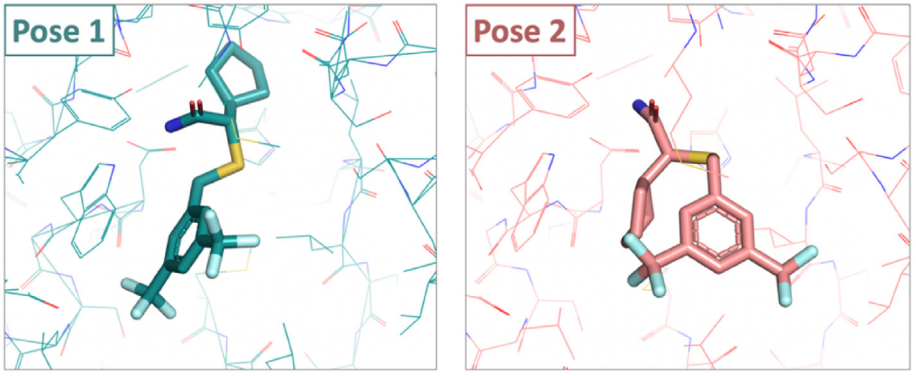

Fig. 1. Two binding modes predicted by docking simulation of **62**. Both shown in the same protein orientation.

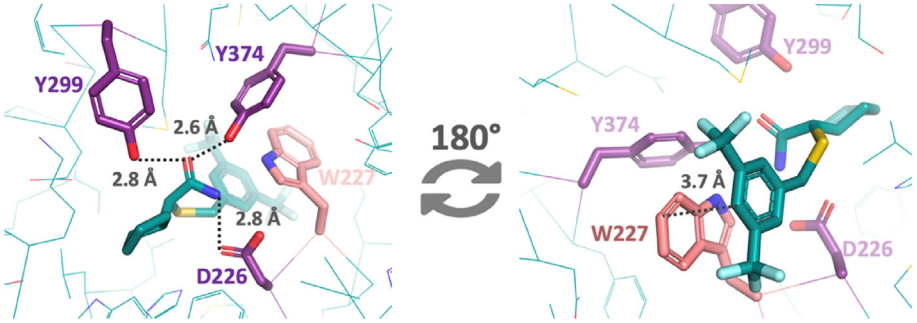

Fig. 2. Key molecular interactions in pose 1. Left: interactions between amide group of **62** with D226, Y299 and Y374 side chain. Right: π−π stacking between **62** and W227. The two images correspond to the same pose rotated 180° to each other.

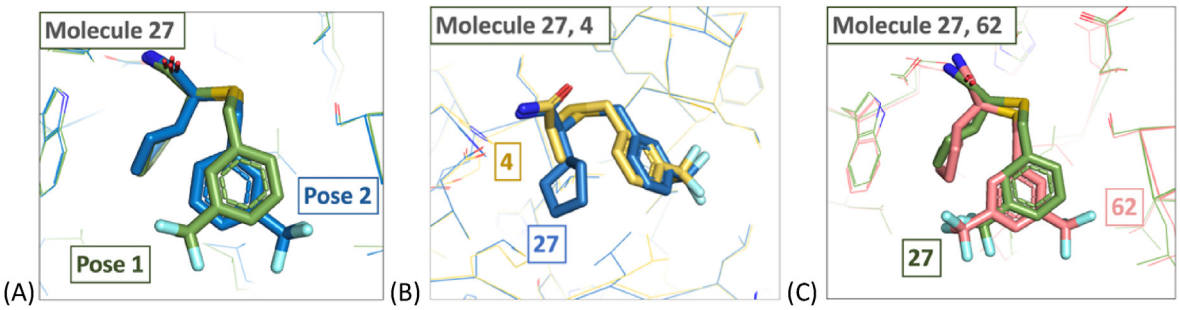

Fig. 3. **(A)** Two binding modes of **27** predicted by docking simulation. **(B)** Comparison between molecule **27** (pose 2) and **4**, shown in blue and yellow respectively. **(C)** Comparison between molecule **27** and **62** binding orientation. Pose 2 of **62** is shown in salmon, pose 1 of molecule **27** is shown in olive. (For interpretation of the references to colour in this figure legend, the reader is referred to the Web version of this article.)

3. Conclusions

In this study, a series of 2-alkylthio acetamide inhibitors of the human microsomal epoxide hydrolase, with IC_{50} values in the low nanomolar range (0.94–11 nM), were obtained. These are over two orders of magnitude more potent than previous primary amine, amide and urea-based mEH inhibitors ($IC_{50} \geq 480$ nM). To better understand structural requirements for potent mEH inhibitors, docking studies were performed with a new homology model of human mEH. Both experimental and docking results point toward the importance of the aryl ring 3–4 bonds away from the acetamide function as well as a bulky aliphatic substituent at the α-position. No interaction with the thioether function was observed, suggesting it can be replaced by a potentially more metabolically stable functionalities, such as a methylene, which will be the subject of ongoing studies.

4. Experimental section

4.1. Reagents and instruments

Many compounds tested as inhibitors or required for synthesis are commercially available and were purchased from one of the following commercial sources: Sigma Aldrich Chemical Co. (Milwaukee, WI), Fisher Scientific (Houston, TX), Eanmine LLC (Monmouth Jct, NJ), Oakwood Chemical (Estill, SC), Chem-Impex Inc (Wood Dale, IL) or Combi-Blocks (San Diego, CA). All reactions were carried out under an atmosphere of dry nitrogen. All chemicals purchased from commercial sources were used as received without further purification. Analytical thin layer chromatography (TLC) was performed on Merck TLC silica gel 60 F254 plates. TLC plates predominantly indicated a single product, following exposure under 254 nm UV light or development using a potassium permanganate stain. Flash chromatography was performed on silica gel (230–400 mesh) from Macherey Nagel. NMR spectra were recorded on Varian VNMRS 600, Inova 400 or Bruker Avance III 800 MHz instruments. Multiplicity is described by the abbreviations b = broad, s = singlet, d = doublet, t = triplet, q = quartet, p = pentet, m = multiplet. Chemical shifts are given in ppm. ^{1}H NMR spectra were referenced to the residual solvent peak at δ = 7.26 ($CDCl_3$). ^{13}C NMR spectra were referenced to the solvent peak at δ = 77.16 ($CDCl_3$). HRMS spectra were recorded on Thermo Electron LTQ-Orbitrap XL Hybrid MS in ESI.

4.2. Chemistry

4.2.1. Synthesis

General procedure of S-alkylation for synthesis of compounds **1**–**28**. A mixture of appropriate 2-bromoacetamide (1 equiv), appropriate thiol (1.1 equiv), K_2CO_3 (1.5 equiv) and DMF (~2 mL/mmol) was stirred at room temperature overnight. Water was added, and the resulting precipitate was filtered. When no precipitate was formed, the product was extracted with EtOAc (3 × 20 mL). Combined organics were dried over $MgSO_4$, filtered and evaporated. Purification by flash column chromatography (EtOAc/hexanes = 10:90 → 40:60 → 50:50) gave pure product, unless noted otherwise.

2-(naphthalen-2-ylthio)propenamide 2. Yield 31%.

^{1}H NMR (600 MHz, $CDCl_3$) δ 7.79 (m, 4H), 7.46 (m, 3H), 6.48 (bs, 1H), 5.53 (bs, 1H), 3.91 (q, J = 7.3 Hz, 1H), 1.61 (d, J = 7.3 Hz, 3H).

HRMS (ESI) calculated m/z 232.0791 (MH+), observed m/z 232.0790 (MH+).

2-((adamantan-1-yl)thio)propenamide 5. Purified by recrystallization from EtOAc/hexanes = 40:60 mixture. Yield 49%.

^{1}H NMR (600 MHz, $CDCl_3$) δ 6.81 (bs, 1H), 6.19 (bs, 1H), 3.41 (q, J = 7.5 Hz, 1H), 2.00 (m, 3H), 1.86 (d, J = 11.8 Hz, 3H), 1.80 (d, J = 11.9 Hz, 3H), 1.65 (d, J = 12.4 Hz, 3H), 1.61 (d, J = 12.3 Hz, 3H), 1.43 (d, J = 7.5 Hz, 3H).

^{13}C NMR (151 MHz, $CDCl_3$) δ 177.9, 46.5, 43.5, 39.5, 36.1, 29.7, 20.7.

HRMS (ESI) calculated m/z 240.1417 (MH+), observed m/z 302.1553 ($[M + HCOONH_4]^+$).

2-((4-bromobenzyl)thio)-2-phenylacetamide 16. Yield 41%.

^{1}H NMR (600 MHz, $CDCl_3$) δ 7.41 (d, J = 8.4 Hz, 2H), 7.34–7.25 (m, 5H), 7.14 (d, J = 8.4 Hz, 2H), 6.35 (bs, 1H), 6.03 (bs, 1H), 4.32 (s, 1H), 3.72 (d, J = 13.6 Hz, 1H), 3.61 (d, J = 13.6 Hz, 1H).

^{13}C NMR (151 MHz, $CDCl_3$) δ 172.2, 136.3, 136.2, 131.8, 130.8, 129.0, 128.4, 128.3, 121.3, 53.6, 36.1.

HRMS (ESI) calculated m/z 336.0052 (MH+), observed m/z 336.0029 (MH+).

2-phenyl-2-((3-(trifluoromethyl)benzyl)thio)acetamide 17. Yield 38%.

^{1}H NMR (600 MHz, $CDCl_3$) δ 7.54–7.42 (m, 4H), 7.37–7.29 (m, 5H), 6.22 (bs, 1H), 5.80 (bs, 1H), 4.36 (s, 1H), 3.85 (d, J = 13.6 Hz, 1H), 3.73 (d, J = 13.6 Hz, 1H).

^{13}C NMR (151 MHz, $CDCl_3$) δ 172.0, 138.2, 136.2, 132.5, 131.4, 131.2, 131.0, 130.7, 129.3, 129.2, 128.6, 128.4, 125.94, 125.92, 125.89, 125.87, 124.43, 124.41, 124.38, 124.36, 53.9, 36.4.

HRMS (ESI) calculated m/z 326.0821 (MH+), observed m/z 326.0796 (MH+).

2-((3-(trifluoromethyl)benzyl)thio)pentanamide 18. Yield 82%.

^{1}H NMR (600 MHz, $CDCl_3$) δ 7.56 (b, 1H), 7.46 (m, 2H), 7.40 (m, 1H), 6.55 (bs, 2H), 6.50 (bs, 1H), 3.78 (m, 2H), 3.13 (t, J = 7.3 Hz, 1H), 1.78 (m, 1H), 1.61 (m, 1H), 1.43 (m, 1H), 1.34 (m, 1H), 0.83 (t, J = 7.4 Hz, 3H).

^{13}C NMR (151 MHz, $CDCl_3$) δ 175.2, 138.5, 132.4, 131.3, 131.1, 130.9, 130.7, 129.1, 126.7, 125.74, 125.72, 125.69, 125.67, 124.9, 124.20, 124.18, 124.15, 124.13, 123.1, 121.3, 49.2, 35.6, 34.3, 20.6, 13.6.

HRMS (ESI) calculated *m/z* 292.0977 (MH+), observed *m/z* 292.0974 (MH+).

2-((3-(trifluoromethyl)benzyl)thio)hexanamide 19. Yield 90%.

^{1}H NMR (600 MHz, $CDCl_3$) δ 7.57 (s, 1H), 7.47 (m, 2H), 7.41 (m, 1H), 6.57 (bs, 1H), 6.49 (bs, 1H), 3.78 (m, 2H), 3.11 (t, J = 7.3 Hz, 1H), 1.81 (m, 1H), 1.63 (m, 1H), 1.38 (m, 1H), 1.30 (m, 1H), 1.23 (m, 2H), 0.83 (t, J = 7.3 Hz, 3H).

^{13}C NMR (151 MHz, $CDCl_3$) δ 175.2, 138.6, 132.4, 131.3, 131.1, 130.9, 130.7, 129.1, 126.8, 125.75, 125.72, 125.70, 125.67, 124.9, 124.21, 124.18, 124.16, 124.13, 123.1, 121.3, 77.2, 49.5, 35.6, 32.1, 29.4, 22.3, 13.8.

HRMS (ESI) calculated *m/z* 306.1134 (MH+), observed *m/z* 306.1134 (MH+).

2-((4-bromobenzyl)thio)-3-methylbutanamide 23. Yield 93%.

^{1}H NMR (600 MHz, $CDCl_3$) δ 7.41 (d, J = 8.4 Hz, 2H), 7.15 (d, J = 8.4 Hz, 2H), 6.56 (bs, 1H), 6.09 (bs, 1H), 3.69 (d, J = 13.4 Hz, 1H), 3.64 (d, J = 13.4 Hz, 1H), 2.93 (d, J = 6.7 Hz, 1H), 2.11 (o, J = 6.6 Hz, 1H), 0.98 (d, J = 6.8 Hz, 3H), 0.95 (d, J = 6.7 Hz, 3H).

^{13}C NMR (151 MHz, $CDCl_3$) δ 174.4, 136.5, 131.8, 130.8, 121.3, 57.2, 35.8, 30.9, 21.0, 19.9.

HRMS (ESI) calculated *m/z* 302.0209 (MH+), observed *m/z* 302.0307 (MH+).

3-methyl-2-((3-(trifluoromethyl)benzyl)thio)butanamide 24. Yield 68%.

^{1}H NMR (600 MHz, $CDCl_3$) δ 7.57 (s, 1H), 7.49 (d, J = 7.8 Hz, 1H), 7.46 (d, J = 7.7 Hz, 1H), 7.41 (t, J = 7.7 Hz, 1H), 6.57 (bs, 1H), 6.26 (bs, 1H), 3.80 (d, J = 13.5 Hz, 1H), 3.75 (d, J = 13.5 Hz, 1H), 2.94 (d, J = 6.7 Hz, 1H), 2.16–2.10 (m, 1H), 0.99 (d, J = 6.8 Hz, 3H), 0.97 (d, J = 6.8 Hz, 3H).

^{13}C NMR (151 MHz, $CDCl_3$) δ 174.4, 138.5, 132.5, 131.4, 131.2, 131.0, 130.8, 129.1, 126.8, 125.80, 125.77, 125.75, 125.72, 124.96, 124.29, 124.26, 124.24, 124.21, 123.2, 121.4, 57.4, 36.0, 30.9, 21.0, 19.8.

HRMS (ESI) calculated *m/z* 292.0977 (MH+), observed *m/z* 292.0983 (MH+).

4-methyl-2-((3-(trifluoromethyl)benzyl)thio)pentanamide 26. Yield 74%.

^{1}H NMR (600 MHz, $CDCl_3$) δ 7.54 (s, 1H), 7.41 (m, 2H), 7.33 (m, 1H), 7.02 (bs, 1H), 6.64 (bs, 1H), 3.75 (s, 2H), 3.16 (t, J = 7.8 Hz, 1H), 1.66 (m, 2H), 1.45 (m, 1H), 0.80 (d, J = 6.5 Hz, 3H), 0.71 (d, J = 6.3 Hz, 3H).

^{13}C NMR (151 MHz, $CDCl_3$) δ 175.6, 138.6, 132.3, 131.1, 130.9, 130.6, 130.4, 128.9, 126.6, 125.60, 125.57, 125.55, 125.52, 124.8, 123.95, 123.93, 123.90, 123.88, 123.0, 121.2, 47.3, 40.8, 35.2, 25.8, 22.3, 21.5.

HRMS (ESI) calculated *m/z* 306.1134 (MH+), observed *m/z* 306.1135 (MH+).

2-cyclopentyl-2-((3-(trifluoromethyl)benzyl)thio)acetamide 27. Yield 32%.

^{1}H NMR (600 MHz, $CDCl_3$) δ 7.59 (s, 1H), 7.51 (d, J = 7.9 Hz, 1H), 7.48 (d, J = 7.9 Hz, 1H), 7.43 (t, J = 7.7 Hz, 1H), 6.30 (bs, 1H), 5.64 (bs, 1H), 3.80 (s, 2H), 3.01 (d, J = 9.1 Hz, 1H), 2.16 (h, J = 8.5 Hz, 1H), 1.85 (m, 1H), 1.77 (m, 1H), 1.62 (m, 2H), 1.53 (m, 2H), 1.37 (m, 1H), 1.26 (m, 1H).

^{13}C NMR (151 MHz, $CDCl_3$) δ 174.5, 138.6, 132.5, 131.4, 131.2, 131.0, 130.8, 129.2, 126.8, 125.84, 125.82, 125.79, 125.77, 125.0, 124.30, 124.27, 124.24, 124.22, 123.2, 121.4, 55.2, 42.2, 35.8, 31.1, 25.2.

HRMS (ESI) calculated *m/z* 318.1134 (MH+), observed *m/z* 318.1137 (MH+).

2-cyclohexyl-2-((3-(trifluoromethyl)benzyl)thio)acetamide 28. Yield 42%.

^{1}H NMR (600 MHz, $CDCl_3$) δ 7.59 (s, 1H), 7.51 (d, J = 7.8 Hz, 1H), 7.47 (d, J = 7.7 Hz, 1H), 7.42 (t, J = 7.8 Hz, 1H), 6.50 (bs, 1H), 5.80 (bs, 1H), 3.81 (d, J = 13.5 Hz, 1H), 3.75 (d, J = 13.5 Hz, 1H), 2.98 (d, J = 6.8 Hz, 1H), 1.91–1.58 (m, 6H), 1.28–0.94 (m, 5H).

^{13}C NMR (151 MHz, $CDCl_3$) δ 174.0, 138.6, 132.5, 131.5, 131.2, 131.0, 130.8, 129.2, 126.8, 125.84, 125.82, 125.79, 125.77, 125.0, 124.33, 124.31, 124.28, 124.26, 123.2, 121.4, 56.6, 40.3, 36.1, 31.4, 30.4, 26.20, 26.15, 26.08.

HRMS (ESI) calculated *m/z* 332.1290 (MH+), observed *m/z* 332.0029 (MH+).

2,3-diphenylpropanamide 29. A mixture of 2,3-diphenylpropanoic acid (403 mg, 1.78 mmol, 1 equiv) and $SOCl_2$ (0.318 g, 2.68 mmol, 1.5 equiv) was refluxed for 3 h. The reaction mixture was cooled down to room temperature, the excess of $SOCl_2$ was evaporated under reduced pressure and the residue was added dropwise to cooled to 0 °C saturated solution of ammonia under vigorous stirring. The resulting precipitate was filtered and dried under vacuum. Yield 0.4 g (quant).

^{1}H NMR (600 MHz, $CDCl_3$) δ 7.28 (m, 5H), 7.20 (t, J = 7.4 Hz, 2H), 7.15 (t, J = 7.3 Hz, 1H), 7.09 (d, J = 7.4 Hz, 2H), 5.58 (bs, 1H), 5.35 (bs, 1H), 3.63 (t, J = 7.5 Hz, 1H), 3.52 (dd, J = 13.7, 7.6 Hz, 1H), 2.98 (dd, J = 13.7, 7.4 Hz, 1H).

^{13}C NMR (151 MHz, $CDCl_3$) δ 175.3, 139.6, 139.5, 129.1, 128.9, 128.4, 128.2, 127.6, 126.4, 54.9, 39.5.

2,2-dicyclohexylacetamide 30. A mixture of 2,2-dicyclohexylacetic acid (2.424 g, 10.8 mmol, 1 equiv) and $SOCl_2$ (3.86 g, 32.5 mmol, 3 equiv) was refluxed for 3 h. The reaction mixture was cooled down to room temperature, the excess of $SOCl_2$ was evaporated under reduced pressure and the residue was added dropwise to cooled to 0 °C saturated solution of ammonia under vigorous stirring. The formed oily precipitate was triturated and washed multiple times with water until it became solid. The solid residue was filtered and dried under vacuum. Yield 1.72 g (71%).

^{1}H NMR (600 MHz, $CDCl_3$) δ 7.83 (s, 1H), 7.17 (s, 1H), 2.05 (t, J = 8.0 Hz, 1H), 1.69 (m, 12H), 1.29–0.92 (m, 10H).

^{13}C NMR (151 MHz, $CDCl_3$) δ 180.9, 57.4, 36.3, 31.4, 29.7, 26.7, 26.6, 26.5.

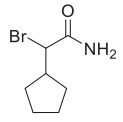

2-bromo-2-cyclopentylacetamide 32. Br_2 (3.6 g, 22.52 mmol, 1.1 equiv) was added to 2-cyclopentylacetyl chloride (3.01 g, 20.48 mmol, 1 equiv) at room temperature. The resulting mixture was refluxed for 2 h, cooled down and added dropwise to the cooled to 0 °C concentrated solution of ammonium hydroxide. The resulting mixture was stirred for additional 15 min and filtered to give the product as a light-brown solid (1.745 g, 41%).

1H NMR (600 MHz, $CDCl_3$) δ 6.29 (bs, 1H), 6.25 (bs, 1H), 4.21 (d, J = 7.6 Hz, 1H), 2.48 (h, J = 8.1 Hz, 1H), 1.88 (m, 1H), 1.81 (m, 1H), 1.63 (m, 4H), 1.40 (m, 2H).

^{13}C NMR (151 MHz, $CDCl_3$) δ 171.8, 56.3, 44.3, 30.9, 30.8, 25.9, 25.3.

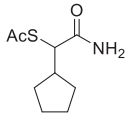

2-amino-1-cyclopentyl-2-oxoethyl ethanethioate 32c. The mixture of 2-bromo-2-cyclopentylacetamide (3.96 g, 19.22 mmol, 1 equiv), AcSK (3.51 g, 30.76 mmol, 1.6 equiv) and DMF (35 mL) was stirred for two days at room temperature, then quenched with water (150 mL) and extracted with EtOAc (3 × 30 mL). Combined organics were dried over $MgSO_4$, filtered and evaporated. The residue was chromatographed (EtOAc/hexanes = 30:70 → 40:60 → 50:50) to give pure product as a pale yellow solid (0.89 g, 23%).

^{1}H NMR (600 MHz, $CDCl_3$) δ 6.40 (bs, 1H), 6.25 (bs, 1H), 3.79 (d, J = 9.9 Hz, 1H), 2.31 (m, 1H), 2.30 (s, 3H), 1.79 (m, 2H), 1.63−1.43 (m, 4H), 1.20 (m, 2H).

^{13}C NMR (151 MHz, $CDCl_3$) δ 196.4, 173.9, 51.6, 39.8, 31.3, 30.7, 30.4, 25.4, 25.1.

2-cyclopentyl-2-mercaptoacetamide 33. A solution of 2-amino-1-cyclopentyl-2-oxoethyl ethanethioate (0.88 g, 4.38 mmol, 1 equiv) and NaOH (10 M in water, 0.88 mL, 8.76 mmol, 2 equiv) in methanol (10 mL) was stirred at room temperature overnight, concentrated to ~3 mL and quenched with water (15 mL) and few drops of hydrochloric acid to bring the pH to ~1. The resulting mixture was extracted with EtOAc (3 × 20 mL). Combined organics were dried over $MgSO_4$, filtered and evaporated to give pure compound as pale yellow solid (0.696 g, quant).

^{1}H NMR (600 MHz, CD_3OD) δ 3.07 (d, J = 10.1 Hz, 1H), 2.18 (dp, J = 9.9, 8.0 Hz, 1H), 1.96 (m, 1H), 1.76 (m, 1H), 1.67 (m, 2H), 1.59 (m, 2H), 1.39 (m, 1H), 1.27 (m, 1H).

^{13}C NMR (101 MHz, $CDCl_3$) δ 175.5, 48.3, 44.4, 31.2, 30.4, 25.7, 25.3.

HRMS (ESI) calculated m/z 160.0791 (MH+), observed m/z 160.0788 (MH+).

General procedure of S-alkylation for synthesis of **34**−**64**. A mixture of 2-cyclopentyl-2-mercaptoacetamide **33** (1 equiv), appropriate benzyl bromide (1.1 equiv), K_2CO_3 (1.5 equiv) and DMF (~2 mL/mmol) was stirred at room temperature overnight. Water was added, and the resulting precipitate was filtered. When no precipitate was formed, the product was extracted with EtOAc (3 × 20 mL). Combined organics were dried over $MgSO_4$, filtered and evaporated. Purification by flash column chromatography (EtOAc/hexanes = 10:90 → 40:60 → 50:50) gave pure product, unless noted otherwise.

2-cyclopentyl-2-((3,5-dichlorobenzyl)thio)acetamide 57. Yield 70%.

^{1}H NMR (400 MHz, CD_3OD) δ 7.33 (m, 2H), 7.31 (m, 1H), 3.80 (d, J = 13.7 Hz, 1H), 3.75 (d, J = 13.7 Hz, 1H), 2.99 (d, J = 10.4 Hz, 1H), 2.18 (m, 1H), 1.87 (m, 1H), 1.77 (m, 1H), 1.69−1.48 (m, 4H), 1.29 (m, 2H).

^{13}C NMR (101 MHz, CD_3OD) δ 177.5, 143.9, 136.0, 128.7, 128.0, 55.6, 42.6, 35.7, 32.1, 26.2, 26.0.

HRMS (ESI) calculated m/z 318.0481 (MH+), observed m/z 318.0485 (MH+).

2-cyclopentyl-2-((3,5-dibromobenzyl)thio)acetamide 58. Yield 85%.

^{1}H NMR (400 MHz, $CDCl_3$) δ 7.55 (t, J = 1.8 Hz, 1H), 7.40 (d, J = 1.7 Hz, 2H), 6.23 (bs, 1H), 5.43 (bs, 1H), 3.68 (s, 2H), 3.03 (d, J = 9.2 Hz, 1H), 2.23−2.10 (m, 1H), 1.91−1.74 (m, 2H), 1.70−1.47 (m, 4H), 1.45−1.19 (m, 2H).

^{13}C NMR (101 MHz, $CDCl_3$) δ 174.1, 141.6, 133.1, 130.9, 123.1, 55.2, 42.2, 35.2, 31.20, 31.19, 25.32, 25.28.

HRMS (ESI) calculated m/z 403.9325 ([M-H]$^-$), observed m/z 441.9059 ([M + K−2H]$^-$)

2-cyclopentyl-2-((3,5-dimethylbenzyl)thio)acetamide 59. Yield 50%.

^{1}H NMR (400 MHz, $CDCl_3$) δ 6.91 (s, 2H), 6.88 (s, 1H), 6.39 (bs, 1H), 5.45 (bs, 1H), 3.68 (s, 2H), 3.10 (d, J = 8.6 Hz, 1H), 2.29 (s, 6H), 2.19 (m, 1H), 1.91−1.70 (m, 2H), 1.68−1.23 (m, 6H).

^{13}C NMR (101 MHz, $CDCl_3$) δ 174.8, 138.3, 137.2, 129.1, 126.9, 55.2, 42.3, 36.5, 31.1, 31.0, 25.3, 25.3, 21.4.

HRMS (ESI) calculated m/z 278.1573 (MH+), observed m/z 278.1574 (MH+).

2-((4-chloro-3-(trifluoromethoxy)benzyl)thio)-2-cyclopentylacetamide 60. Yield 65%.

^{1}H NMR (400 MHz, $CDCl_3$) δ 7.39 (d, J = 8.2 Hz, 1H), 7.32 (s, 1H), 7.18 (dd, J = 8.2, 2.1 Hz, 1H), 6.25 (bs, 1H), 5.82 (bs, 1H), 3.72 (s, 2H), 2.96 (d, J = 9.2 Hz, 1H), 2.14 (m, 1H), 1.89−1.70 (m, 2H), 1.68−1.44 (m, 4H), 1.41−1.17 (m, 2H).

^{13}C NMR (101 MHz, $CDCl_3$) δ 174.5, 145.3, 138.4, 131.1, 128.6, 126.3, 124.4, 123.2, 121.9, 119.3, 116.7, 55.0, 42.1, 35.2, 31.19, 31.16, 25.27, 25.22.

HRMS (ESI) calculated m/z 368.0693 (MH+), observed m/z 368.0697 (MH+).

2-((3,5-bis(trifluoromethyl)benzyl) thio)-2-cyclopentylacetamide 62. Yield quant.

^{1}H NMR (600 MHz, $CDCl_3$) δ 7.78 (s, 2H), 7.76 (s, 1H), 6.23 (bs, 1H), 6.11 (bs, 1H), 3.87 (s, 2H), 2.99 (d, J = 9.4 Hz, 1H), 2.15 (m, 1H), 1.85 (m, 1H), 1.78 (m, 1H), 1.67−1.47 (m, 4H), 1.35 (m, 1H), 1.26 (m, 1H).

^{13}C NMR (151 MHz, $CDCl_3$) δ 174.4, 140.4, 132.3, 132.1, 131.8, 131.6, 129.26, 129.24, 126.0, 124.2, 122.4, 121.44, 121.41, 121.39, 121.36, 121.34, 120.6, 55.29, 42.0, 35.3, 31.21, 31.19, 25.25, 25.18.

HRMS (ESI) calculated m/z 386.1008 (MH+), observed m/z 386.1007 (MH+).

2-cyclopentyl-2-((1-(3-(trifluoromethyl)phenyl)ethyl)thio) acetamide 63. Yield 73% (mixture of diastereomers).

^{1}H NMR (400 MHz, $CDCl_3$) δ 7.64 (s, 0.5H), 7.58 (s, 0.5H), 7.50 (m, 2H), 7.42 (m, 1H), 6.36 (bs, 0.5H), 6.17 (bs, 0.5H), 5.87 (bs, 0.5H), 5.62 (bs, 0.5H), 4.05 (q, J = 6.6 Hz, 0.5H), 4.00 (q, J = 7.1 Hz, 0.5H), 3.17 (d, J = 8.6 Hz, 0.5H), 2.66 (d, J = 8.6 Hz, 0.5H), 2.20−2.03 (m, 1H), 1.86−1.35 (m, 6H), 1.65 (d, J = 7.0 Hz, 1.5H), 1.56 (d, J = 7.1 Hz, 1.5H), 1.34−1.22 (m, 2H).

^{13}C NMR (101 MHz, $CDCl_3$) δ 174.99, 174.80, 144.58, 144.37, 131.66, 131.56, 131.34, 131.24, 131.08, 131.07, 131.02, 130.92, 130.83, 130.82, 130.70, 130.60, 129.22, 129.14, 128.23, 128.19, 125.52, 125.48, 124.36, 124.35, 124.33, 124.31, 124.19, 124.15, 124.11, 124.07, 124.04, 124.00, 123.96, 122.81, 122.77, 120.10, 120.06, 55.50, 54.89, 44.64, 44.22, 42.60, 42.22, 31.05, 31.03, 30.95, 30.84, 25.27, 25.26, 25.17, 25.16, 22.95, 22.40.

HRMS (ESI) calculated m/z 332.1290 (MH+), observed m/z 332.1296 (MH+).

General procedure for the synthesis of amides in Tables 3−4 and Table SI-1.

Mixed anhydride of the acetic and formic acid was prepared by heating the mixture of Ac_2O (1 equiv) and HCOOH (2 equiv) at 60 °C for 2 h. To accelerate the screening process, most of the synthesized amides were tested as crude products as described below. Appropriate anhydride (1 equiv) was added to the mixture of amine (1 equiv), Et_3N (3 equiv) and DCM (1 mL) in 2 mL screwtop vial at room temperature. All reactions were performed on 30−100 μmol scale. The vial was vortexed and left overnight at room temperature. The solvent was evaporated under a gentle stream of nitrogen and the residue was dissolved in appropriate amount of DMSO to obtain 10 mM solution of the amide (assuming quantitative yield). The resulting solution was used in the mEH inhibition assay. Blanc reaction lacking the primary amine (i.e. all the reagents and conditions are the same, except for addition of the primary amine) performed in a similar way as described above did not show any inhibition of the mEH.

N-dodecylmethanesulfonamide 70. Yield 60%.

^{1}H NMR (600 MHz, $CDCl_3$) δ 4.19 (bs, 1H), 3.13 (q, J = 6.8 Hz, 2H), 2.95 (s, 3H), 1.57 (m, 2H), 1.38−1.20 (m, 18H), 0.88 (t, J = 6.9 Hz, 3H).

^{13}C NMR (151 MHz, $CDCl_3$) δ 43.5, 40.5, 32.1, 30.3, 29.77, 29.76, 29.69, 29.63, 29.5, 29.3, 26.7, 22.8, 14.3.

HRMS (ESI) calculated *m/z* 262.1846 ([M-H]$^-$), observed *m/z* 340.1606 ([M + NH_4Ac]$^-$)

N-dodecyl-1,1,1-trifluoromethanesulfonamide 71. Yield 65%.

^{1}H NMR (600 MHz, $CDCl_3$) δ 4.95 (bs, 1H), 3.29 (q, J = 6.7 Hz, 2H), 1.60 (p, J = 7.2 Hz, 2H), 1.37−1.22 (m, 18H), 0.88 (t, J = 6.9 Hz, 3H).

^{13}C NMR (151 MHz, $CDCl_3$) δ 171.5, 123.0, 120.9, 118.7, 116.6, 44.7, 32.1, 30.3, 29.74, 29.64, 29.55, 29.48, 29.1, 26.4, 22.8, 14.3.

HRMS (ESI) calculated *m/z* 316.1564 ([M-H]$^-$), observed *m/z* 316.1541 ([M-H]$^-$)

2-bromopentanamide 122. A mixture of 2-bromopentanoic acid (1.81 g, 10 mmol, 1 equiv) and $SOCl_2$ (3.57 g, 30 mmol, 3 equiv) was heated at 70 °C for 3 h. The reaction mixture was then cooled down and the excess of $SOCl_2$ was evaporated under vacuum. The residue was added dropwise to the cooled to 0 °C concentrated solution of ammonium hydroxide. The resulting mixture was stirred for additional 15 min and filtered to give the product as a light-brown solid (0.61 g, 34%).

^{1}H NMR (600 MHz, $CDCl_3$) δ 6.32 (bs, 1H), 5.79 (bs, 1H), 4.30 (dd, J = 8.3, 5.1 Hz, 1H), 2.10 (m, 1H), 2.00 (m, 1H), 1.56 (m, 1H), 1.48 (m, 1H), 0.96 (t, J = 7.4 Hz, 3H).

^{13}C NMR (151 MHz, $CDCl_3$) δ 171.6, 50.7, 37.9, 20.6, 13.4.

2-bromo-2-cyclohexylacetamide 133. A solution of $NaNO_2$ (3.53 g, 51.2 mmol, 1.6 equiv) in water (30 mL) was slowly added to the cooled to 0 °C mixture of 2-amino-2-cyclohexylacetic acid (5 g, 32 mmol, 1 equiv), 48% HBr in water (48.6 g, 288 mmol, 9 equiv) and water (10 mL). The reaction mixture was stirred for 2 h and extracted with EtOAc (3 × 20 mL). Combined extracts were dried over $MgSO_4$, filtered and evaporated to give crude 2-bromo-2-cyclohexylacetic acid which was used in the next step without purification.

A mixture of crude 2-bromo-2-cyclohexylacetic acid and $SOCl_2$ (14.28 g, 120 mmol, 3 equiv) was refluxed for 3 h, cooled down and added dropwise to the cooled to 0 °C concentrated solution of ammonium hydroxide. The resulting mixture was stirred for additional 15 min and filtered to give the product as a light-brown solid (6.102 g, 87%).

^{1}H NMR (600 MHz, $CDCl_3$) δ 6.55 (bs, 1H), 6.46 (bs, 1H), 4.18 (d, J = 5.6 Hz, 1H), 1.98−1.61 (m, 6H), 1.26 (m, 3H), 1.15 (m, 2H).

^{13}C NMR (151 MHz, $CDCl_3$) δ 171.8, 58.5, 41.8, 31.1, 29.3, 26.0, 25.9, 25.8.

4.3. Biological evaluation

a) Measurement of mEH inhibition using a fluorometric assay

This was the primary assay utilized to determine the IC_{50} for all the inhibitors. It is derived from a previously described protocol used to measure sEH inhibition [15], modified and optimized for mEH. It involves an α-cyanocarbonate epoxide (CMNGC) substrate, which yields a strong fluorescent signal upon hydrolysis by mEH. The detailed, step by step protocol is described in the supplementary information.

b) Radiometric assay for mEH activity using [^{3}H] cis-stilbene oxide (c-SO)

This was the secondary assay utilized to validate the potency of compound **62.** It is derived from a previously described assay used to measure sEH activity in tissue extracts, using [^{3}H] trans-stilbene oxide (t-SO) [15], modified and optimized for mEH. It is based on the differential partitioning of the epoxide substrate and the more polar 1,2 diol product in the organic and aqueous fractions, respectively. The detailed, step by step protocol is described in the supplementary information.

4.4. Homology modeling

No crystal structure of mEH is currently available. In order to predict the protein structure of mEH, homology modeling was carried out using the RosettaCM protocol [23]. While a homology model of mEH was reported previously [24], here we applied a homology modeling method that incorporates geometric constraints on catalytic residues [25] in an attempt to increase the accuracy of the prediction of the active site structure.

To select templates for homology modeling, a HMMER [26] search was performed and six sequences were identified as high sequence identity templates (4I19, 5F4Z,1QO7, 5BOV, 5CW2, 1EHY, see SI for more information). A multiple sequence alignment was carried out to correlate sequence position to structure using Promals3D [27]. Structural fragment sets were generated and applied during the modeling to sample the unaligned regions with standard methods [28]. During multi-template fragment based modeling with RosettaCM, evolutionary constraints were used to enhance sampling [29]. Geometric constraints on three residues − D226, Y299 and Y374 − were applied during the homology modeling: D226 acts as the nucleophile that attacks the epoxide ring, while Y299 and Y374 are important for binding of the substrate epoxy group oxygen (i.e., they comprise an oxyanion hole) [19]. Thus, these residues were constrained in space during the modeling to enforce the catalytic residues to maintain a viable arrangement (see SI for details). Using this protocol, 5000 models of mEH were generated and the top scored model was selected as a starting point for ligand docking.

4.5. Docking

A library of conformations for each tested molecule was generated with Spartan '16 using molecular mechanics (MMFF) [30]. Conformers within 5 kcal/mol of the lowest energy conformer were retained for docking. These conformers were then optimized with Gaussian09 using the ωB97XD/6-31+G(d,p) density functional theory method in the gas phase [22].

To investigate the binding mode of potent inhibitors, docking simulations were performed with the Rosetta Molecular Modeling Suite [31][32]. The low energy homology model generated from RosettaCM was used as the protein model to which the conformer library was docked. Docking runs were carried out with chemically meaningful constraints [33,34]. Two types of constraints were applied: 1) Chemistry constraints. 2) Triad Constraints. The former defines the constraints between the inhibitor with catalytic triad residues: 299Y, 374Y and 226D. The later defines constraints between catalytic residues including 404E, 431H, 374Y, 299Y, 226D. Geometric constraint values were determined using a close homologue of mEH (PDB: 3G0I, see SI for Details). For each tested molecule, 2500 docking simulations were conducted, and the resulting poses were filtered on the basis of constraint satisfaction, total energy and interface energy (structures that were within one standard deviation or lower from the mean energy were retained). The top scoring models were further analyzed to evaluate the predicted intermolecular interactions at the protein-ligand interface.

Declaration of competing interest

The authors declare that they have no known competing financial interests or personal relationships that could have appeared to influence the work reported in this paper.

Acknowledgements and Funding

This study was supported by grants from the National Institutes of Health (R35 ES030443, R01 DK107767 and R01 GM076324-11), the National Institute of Environmental Health Sciences Superfund Research Program P42 ES004699, the National Science Foundation (award numbers 1827246, 1805510 and 1627539) and the Rosetta Commons. DJT and YZ gratefully acknowledge computation support from the US National Science Foundation's XSEDE program. The content is solely the responsibility of the authors and does not necessarily represent the official views of the National Institutes of Health or National Science Foundation.

Appendix A. Supplementary data

Supplementary data to this article can be found online at https://doi.org/10.1016/j.ejmech.2020.112206.

References

[1] R. Václavíková, D.J. Hughes, P. Souček, Microsomal epoxide hydrolase 1 (EPHX1): gene, structure, function, and role in human disease, Gene 571 (1) (2015) 1–8, https://doi.org/10.1016/j.Gene.2015.07.071.
[2] B.D. Hammock, D.N. Loury, D.E. Moody, B. Ruebner, R. Baselt, K.M. Milam, P. Volberding, A. Ketterman, R. Talcott, A methodology for the analysis of the preneoplastic antigen, Carcinogenesis 5 (11) (1984) 1467–1473, https://doi.org/10.1093/carcin/5.11.1467.
[3] A.A. El-Sherbeni, A.O. El-Kadi, The role of epoxide hydrolases in Health and disease, Arch. Toxicol. 88 (2014) 2013–2032, https://doi.org/10.1007/s00204-014-1371-y.
[4] F. Toselli, M. Fredenwall, P. Svensson, X.-Q. Li, A. Johansson, L. Weidolf, M.A. Hayes, Oxetane substrates of human microsomal epoxide hydrolase, Drug Metab. Dispos. 45 (8) (2017) 966–973, https://doi.org/10.1124/dmd.117.076489.
[5] F. Toselli, M. Fredenwall, P. Svensson, X.-Q. Li, A. Johansson, L. Weidolf, M.A. Hayes, Hip to Be square: oxetanes as design elements to alter metabolic pathways, J. Med. Chem. 62 (2019) 7383–7399, https://doi.org/10.1021/acs.jmedchem.9b00030.
[6] M.L. Edin, B.G. Hamedani, A. Gruzdev, J.P. Graves, F.B. Lih, S.J. Arbes, R. Singh, A.C.O. Leon, J.A. Bradbury, L.M. DeGraff, et al., Epoxide hydrolase 1 (EPHX1) hydrolyzes epoxyeicosanoids and impairs cardiac recovery after ischemia, J. Biol. Chem. 293 (9) (2018) 3281–3292, https://doi.org/10.1074/jbc.RA117.000298.
[7] G.T. Brooks, A. Harrison, S.E. Lewis, Cyclodiene epoxide ring hydration by microsomes from mammalian liver and houseflies, Biochem. Pharmacol. 19 (1) (1970) 255–273, https://doi.org/10.1016/0006-2952(70)90346-1.
[8] F. Oesch, Mammalian epoxide hydrases: inducible enzymes catalysing the inactivation of carcinogenic and cytotoxic metabolites derived from aromatic and olefinic compounds, Xenobiotica 3 (5) (1973) 305–340, https://doi.org/10.3109/00498257309151525.
[9] G.T. Brooks, Epoxide hydratase as a modifer of biotransformation and biological activity, Gen. Pharmacol. 8 (4) (1977) 221–226, https://doi.org/10.1016/0306-3623(77)90016-7.
[10] C. Morisseau, J.W. Newman, D.L. Dowdy, M.H. Goodrow, B.D. Hammock, Inhibition of microsomal epoxide hydrolases by ureas, amides, and amines, Chem. Res. Toxicol. 14 (4) (2001) 409–415, https://doi.org/10.1021/tx0001732.
[11] C. Morisseau, J.W. Newman, C.E. Wheelock, T. Hill, D. Morin, A.R. Buckpitt, B.D. Hammock, Development of metabolically stable inhibitors of mammalian microsomal epoxide hydrolase, Chem. Res. Toxicol. 21 (4) (2008) 951–957, https://doi.org/10.1021/tx700446u.
[12] S.G. Kamita, K. Yamamoto, M.M. Dadala, K. Pha, C. Morisseau, A. Escaich, B.D. Hammock, Cloning and characterization of a microsomal epoxide hydrolase from Heliothis virescens, Insect Biochem. Mol. Biol. 43 (3) (2013) 219–228, https://doi.org/10.1016/j.ibmb.2012.12.002.
[13] B. Meunier, S.P. de Visser, S. Shaik, Mechanism of oxidation reactions catalyzed by cytochrome P450 enzymes, Chem. Rev. 104 (9) (2004) 3947–3980, https://doi.org/10.1021/cr020443g.
[14] S.K. Krueger, D.E. Williams, Mammalian flavin-containing monooxygenases: structure/function, genetic polymorphisms and role in drug metabolism, Pharmacol. Ther. 106 (3) (2005) 357–387, https://doi.org/10.1016/J.PHARMTHERA.2005.01.001.
[15] C. Morisseau, B.D. Hammock, Measurement of Soluble Epoxide Hydrolase (SEH) Activity. In Current Protocols in Toxicology vol. 33, John Wiley & Sons, Inc., Hoboken, NJ, USA, 2007, https://doi.org/10.1002/0471140856.tx0423s33, 4.23.1-4.23.18.
[16] O. Spiegelstein, D.L. Kroetz, R.H. Levy, B. Yagen, S.I. Hurst, M. Levi, A. Haj-Yehia, M. Bialer, Structure activity relationship of human microsomal epoxide hydrolase inhibition by amide and acid analogues of valproic acid, Pharm. Res. (N. Y.) 17 (2) (2000) 216–221, https://doi.org/10.1023/A:1007577600088.
[17] C.M. Breneman, K.B. Wiberg, Determining atom-centered monopoles from molecular electrostatic potentials. The need for high sampling density in formamide conformational analysis, J. Comput. Chem. 11 (3) (1990) 361–373, https://doi.org/10.1002/jcc.540110311.
[18] M.J. Frisch, G.W. Trucks, H.B. Schlegel, G.E. Scuseria, M.A. Robb, J.R. Cheeseman, G. Scalmani, V. Barone, G.A. Petersson, H. Nakatsuji, et al., Gaussian 09, Revision A.02, Gaussian, Inc (2016).
[19] C. Morisseau, B.D. Hammock, Epoxide hydrolases: mechanisms, inhibitor designs, and biological roles, Annu. Rev. Pharmacol. Toxicol. 45 (1) (2004) 311–333, https://doi.org/10.1146/annurev.pharmtox.45.120403.095920.
[20] A.V. Marenich, C.J. Cramer, D.G. Truhlar, Universal solvation model based on solute Electron density and on a continuum model of the solvent defined by the bulk dielectric constant and atomic surface tensions, J. Phys. Chem. B 113 (18) (2009) 6378–6396, https://doi.org/10.1021/jp810292n.
[21] J. Da Chai, M. Head-Gordon, Long-range corrected Hybrid density functionals with damped atom-atom dispersion corrections, Phys. Chem. Chem. Phys. 10 (44) (2008) 6615–6620, https://doi.org/10.1039/b810189b.
[22] M.J. Frisch, G.W. Trucks, H.B. Schlegel, G.E. Scuseria, M.A. Robb, J.R. Cheeseman, G. Scalmani, V. Barone, B. Mennucci, G.A. Petersson, et al., Gaussian 03, Revision C. 02, Gaussian, Inc., 2013, pp. 1–20.
[23] Y. Song, F. Dimaio, R.Y.R. Wang, D. Kim, C. Miles, T. Brunette, J. Thompson, D. Baker, High-resolution comparative modeling with RosettaCM, Structure 21 (10) (2013) 1735–1742, https://doi.org/10.1016/j.str.2013.08.005.
[24] P. Saenz-Méndez, A. Katz, M.L. Pérez-Kempner, O.N. Ventura, M. Vázquez, Structural insights into human microsomal epoxide hydrolase by combined homology modeling, molecular dynamics simulations, and molecular docking calculations, Proteins Struct. Funct. Bioinf. 85 (4) (2017) 720–730, https://doi.org/10.1002/prot.25251.
[25] S.J. Bertolani, J.B. Siegel, A new benchmark illustrates that integration of geometric constraints inferred from enzyme reaction Chemistry can increase enzyme active site modeling accuracy, PLoS One 14 (4) (2019), e0214126, https://doi.org/10.1371/journal.pone.0214126.
[26] S.C. Potter, A. Luciani, S.R. Eddy, Y. Park, R. Lopez, R.D. Finn, HMMER web server: 2018 update, Nucleic Acids Res. 46 (W1) (2018) W200–W204, https://doi.org/10.1093/nar/gky448.
[27] J. Pei, N.V. Grishin, PROMALS3D: multiple protein sequence alignment enhanced with evolutionary and three-dimensional structural information, Methods Mol. Biol. 1079 (2014) 263–271, https://doi.org/10.1007/978-1-62703-646-7_17.
[28] D. Gront, D.W. Kulp, R.M. Vernon, C.E.M. Strauss, D. Baker, Generalized fragment picking in Rosetta: design, protocols and applications, PLoS One 6 (8) (2011), e23294, https://doi.org/10.1371/journal.pone.0023294.
[29] J. Thompson, D. Baker, Incorporation of evolutionary information into Rosetta comparative modeling, Proteins Struct. Funct. Bioinf. 79 (8) (2011) 2380–2388, https://doi.org/10.1002/prot.23046.
[30] Y. Shao, L.F. Molnar, Y. Jung, J. Kussmann, C. Ochsenfeld, S.T. Brown, A.T.B. Gilbert, L.V. Slipchenko, S.V. Levchenko, D.P. O'Neill, et al., Advances in methods and algorithms in a modern quantum chemistry program package, Phys. Chem. Chem. Phys. 8 (2006) 3172–3191, https://doi.org/10.1039/b517914a.
[31] A. Leaver-Fay, M. Tyka, S.M. Lewis, O.F. Lange, J. Thompson, R. Jacak, K.W. Kaufman, P.D. Renfrew, C.A. Smith, W. Sheffler, et al., ROSETTA3: an object-oriented software suite for the simulation and design of macromolecules. Methods Enzymol. 487 (2011) 545–574, https://doi.org/10.1016/B978-0-12-381270-4.00019-6.
[32] R.F. Alford, A. Leaver-Fay, J.R. Jeliazkov, M.J. O'Meara, F.P. DiMaio, H. Park, M.V. Shapovalov, P.D. Renfrew, V.K. Mulligan, K. Kappel, et al., The Rosetta all-atom energy function for macromolecular modeling and design, J. Chem. Theor. Comput. 13 (6) (2017) 3031–3048, https://doi.org/10.1021/acs.jctc.7b00125.
[33] T.E. O'Brien, S.J. Bertolani, D.J. Tantillo, J.B. Siegel, Mechanistically informed predictions of binding modes for carbocation intermediates of a sesquiterpene synthase reaction, Chem. Sci. 7 (7) (2016) 4009–4015, https://doi.org/10.1039/c6sc00635c.
[34] T.E. O'Brien, S.J. Bertolani, Y. Zhang, J.B. Siegel, D.J. Tantillo, Predicting productive binding modes for substrates and carbocation intermediates in terpene synthases - bornyl diphosphate synthase as a representative case, ACS Catal. 8 (4) (2018) 3322–3330, https://doi.org/10.1021/acscatal.8b00342.